



The Cr impurity effect on the optical properties of the Ti₂N graphene-like materials: a DFT study

Mohammad Reza Khodarahmi¹ · Arash Boochani¹ · Heidar Khosravi¹

Received: 26 July 2019 / Accepted: 27 August 2019 / Published online: 13 September 2019
© The Author(s) 2019

Abstract

The electronic and optical behaviors of the Ti₂N graphene-like (GL) materials under the Cr impurity have been investigated based on DFT framework. The band structure and density of state (DOS) diagrams indicated that Ti₂N:Cr GL has the magnetic metallic behavior about $3.2\mu_B$. The density levels around the Fermi level in the band structure and the continuous DOS of under-Fermi to upper refer to the metallic nature of this compound. Adding Cr impurity has increased the metallic behavior so that the real and imaginary parts of dielectric functions have the red shift and their static values shifted to an infinite amount. Also, other optical parameters such as refraction, extinction and Eloss have been studied from the dielectric functions.

Keywords DFT · Ti₂N:Cr GL · Electronic properties · Optical properties

Introduction

After the discovery of graphene [1], most efforts have been made to find new two-dimensional (2D) materials [2–5]. 2D materials have unique physical properties which are attractive for electronic, thermal, magnetic and optical applications. Commonly, two main categories were defined for the 2D materials: graphene-based (GB) and graphene-like (GL) materials. The GBs contain new materials such as graphene, fluorographene and graphene oxides, and the GL materials (free-standing carbon-free 2D crystals) WS₂ and Co₂VAI [5–11].

Indubitably, most GL compound candidates have the layered compound as graphite, which encompasses sharp anisotropic structure so that they have strong inter-atomic bonds inside each layer against very weak van der Waals-type bonding between neighboring sheets.

So, the 2D compounds with mechanical exfoliation (micro-mechanical cleavage) and various chemical approaches [12–17] can be synthesized and investigated for GL classes. The probability of being the GL compounds in the isotropic crystals with a 3D-like system of directional

inter-atomic bonds is more than other compounds. For the first time, the graphene-like carbides were proposed in the ternary MAX phases [18]. A set of 2D GL compositions of MXene have been reported [19–25] which were obtained from their 3D MAX phases, where M belongs to the transition d metals, X stands for C or N, and A denotes Cd, Al, Ga, In, Tl, Si, Ge, Sn, Pb, P, As or S. The 2D GL titanium carbides and nitrides Tin + 1Xn (X = C, N, n = 1, 2, 3) are obtained from 3D Tin + 1AXn (A = Al..., X = C, N) [26, 27] with hexagonal lattice by p63mmc space group [19, 28, 29].

Accordingly, the MAX (Tin + 1AXn) structure is a close-pack in-plane hexagonal MX inner layer of A atoms along the *c*-axis. The M–X bonds have the strong covalent bonds, where the inter-atomic A–A bonds and interlayer M–A ones are the van der Waals ones. These weak bonding could easily be broken in chemical reactions (for instance, Ti₃AlC₂ + 3HF = AlF₃ + 3/2H₂ + Ti₃C₂) leaving a 2D hexagonal MX known as monolayer MXene [30, 31]. The 3D Tin + 1AXn ceramics have interesting physical properties such as low density, high melting point and rust resistance [32–36].

The electronic and optical studies reported that these compounds are good candidates for anti-ultraviolet ray coating materials as well as high-temperature apparatus. Recently, the physical properties of Tin + 1Xn (X = C, N; n = 1, 2, 3) 2D GL such as structural, electronic and optical properties have been investigated, all implicating a high

✉ Arash Boochani
arash_bch@yahoo.com

¹ Department of Physics, Kermanshah Branch, Islamic Azad University, Kermanshah, Iran



potential for application in nano-technology [37]. Some theoretical and experimental works were focused on the electrical resistivity and conduction, elastic constants [38] and their application in the Li-ion batteries [39–45].

Addition of impurities is a good technique to engineer the physical behavior of the materials, especially the magnetic metals. For the first time, we added the Cr atom to the Ti_2N GL nano-sheet and calculated the electronic and optical behavior of the $\text{Ti}_2\text{N}:\text{Cr}$ GL. This paper is organized as follows: the next section gives computational details, followed by which part and results are collected and the final section concludes the paper.

Computational methods

The electronic and optical properties of the $\text{Ti}_2\text{N}:\text{Cr}$ GL have been investigated based on the density functional theory (DFT) framework and Wien2K code [46, 47]. The calculations are done by full-potential augmented plane wave (FP-LAPW) and the exchange potential is approximated by GGA [48]. The super-cell structure of the $\text{Ti}_2\text{N}:\text{Cr}$ GL (Fig. 1) was optimized by mini-position command and the atomic forces on its atomic positions were optimized to 0.1 Reyd/a.u. The input parameters such as RKmax, KPoint, lmax and Gmax were optimized based on the total energy to 7.5, 400, 10 and 13.5, respectively. Also, the optical calculations are approximated by random phase approximations (RPA) using KPoint of 700 in this part.

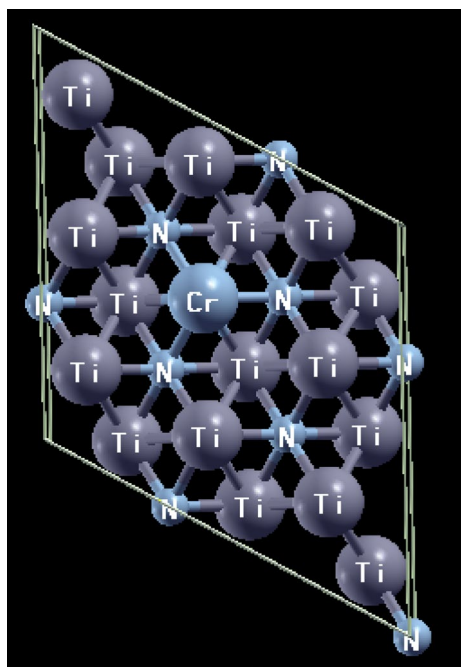


Fig. 1 The $\text{Ti}_2\text{N}:\text{Cr}$ GL super cell, drawn by xcrystden code

Results and discussion

Electronic properties

The band structure diagrams contain important information about the electronic and optical properties of materials. The $\text{Ti}_2\text{N}:\text{Cr}$ GL band structure along the symmetry directions of the first Brillouin zone for two spin channels is depicted. The Cr impurity belongs to the transition metals with the half-full d orbital replaced with Ti atom, with its electronic structure similar to Ti. The pure Ti_2N GL has no magnetic behavior; therefore, we added the Cr impurity to it, the magnetic moment emerged in the $\text{Ti}_2\text{N}:\text{Cr}$ GL case. The band structures of the $\text{Ti}_2\text{N}:\text{Cr}$ GL of the two up and down spin channels are depicted in Fig. 2 for two large and little energy ranges. It is shown that a set of the energy levels are located in the -7 to -5 eV range, which has no magnetic behavior and no sensitivity to the external magnetic field. An energy gap of 3 eV exists in the -5 to -2 eV interval in the valance area which is independent of the external magnetic fields. But in the -2 eV to 8eV range the energy levels are intertwined, continuously, implying to the high metallic nature of this compound. For investigating the magnetic behavior of this composition, the band structure repainted around the Fermi level -2 to 2 eV. It is shown that under the external magnetic field the splitting occurred in the up spin and the level shapes are completely different in the two mentioned spins. The curve slopes of the levels show completely different behavior in the two mentioned spins. The curve gradients of the up spin are greater than down spin especially along $\Gamma \rightarrow \text{M}$ and $\text{K} \rightarrow \Gamma$, respectively; so, the electron mobility is higher in the up spin than down spin, implying the magnetic metallic nature of $\text{Ti}_2\text{N}:\text{Cr}$ GL.

The density of states (DOS) is another useful tool for studying the electronic and optical properties of materials. The DOS diagrams of the $\text{Ti}_2\text{N}:\text{Cr}$ GL composition for the up and down spins are depicted in Fig. 3. Little anisotropy of DOS at the -7 to -5 eV interval and also at the lower and upper Fermi levels has been shown. The partial DOS of the $\text{Ti}_2\text{N}:\text{Cr}$ GL atoms is depicted in the (b, c and d) panels for Ti, N and Cr atoms, respectively. It is shown that the main magnetic anisotropy at the Fermi level originated from the Ti- and Cr- d orbitals and then their p orbitals. Also, the Ti- and Cr- d orbitals around at the valance band refer to their bonding. The continuous bands in the lower to upper Fermi level imply very good electronic conductivity in the two mentioned spins. So, we expect this compound to have good optical sensitivity in the infrared and visible areas.

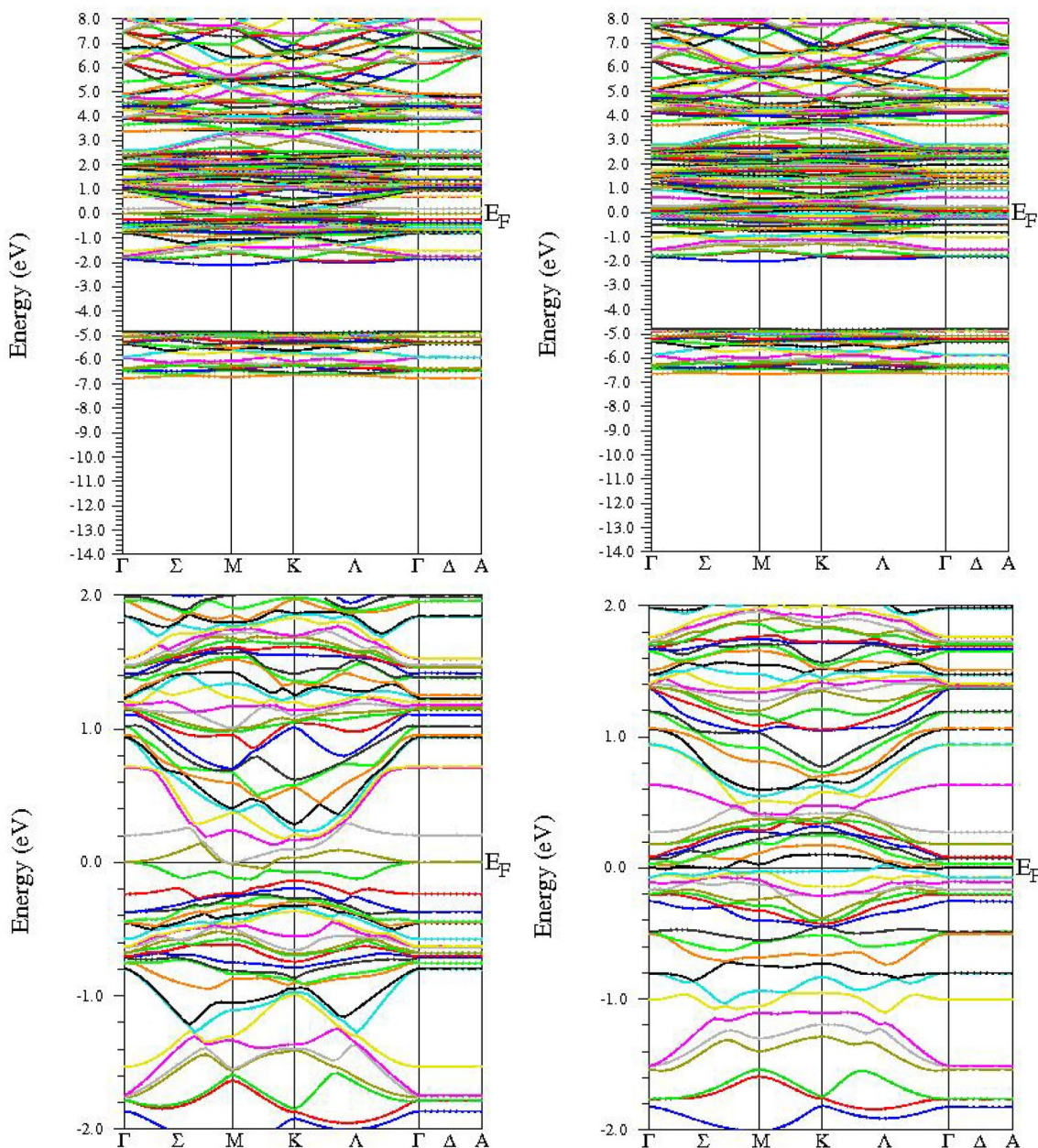


Fig. 2 The band structure of the $Ti_2N:Cr$ GL in the two up and down spins (left and right) for two large and low-energy ranges

Optical property

Based on the metallic properties of the last section, we expect $Ti_2N:Cr$ GL to be a good candidate for optical applications in the infrared and visible areas. Accordingly, the optical coefficients were calculated based on the RPA method by selecting the 400 K point in the first Brillouin zone. In the first step, the imaginary part of the dielectric tensor is obtained and based on the Kramers–Kronig relations the real part of the dielectric is extracted [49, 50]. All

other optical parameters such as absorption, energy loss functions (Eloss), reflection, refraction and extinction can be extracted from the dielectric tensor. Based on the metallic nature of the $Ti_2N:Cr$ GL compound, the optical calculations were done based on the intraband framework. The interband transition of the imaginary part of dielectric function ($Im \epsilon(\omega)$) is formulated as follows, which includes the summation of interband transitions from the occupied valence levels ($|\psi_k^{V_n}\rangle$) to unoccupied conduction ones ($|\psi_k^{C_n}\rangle$):

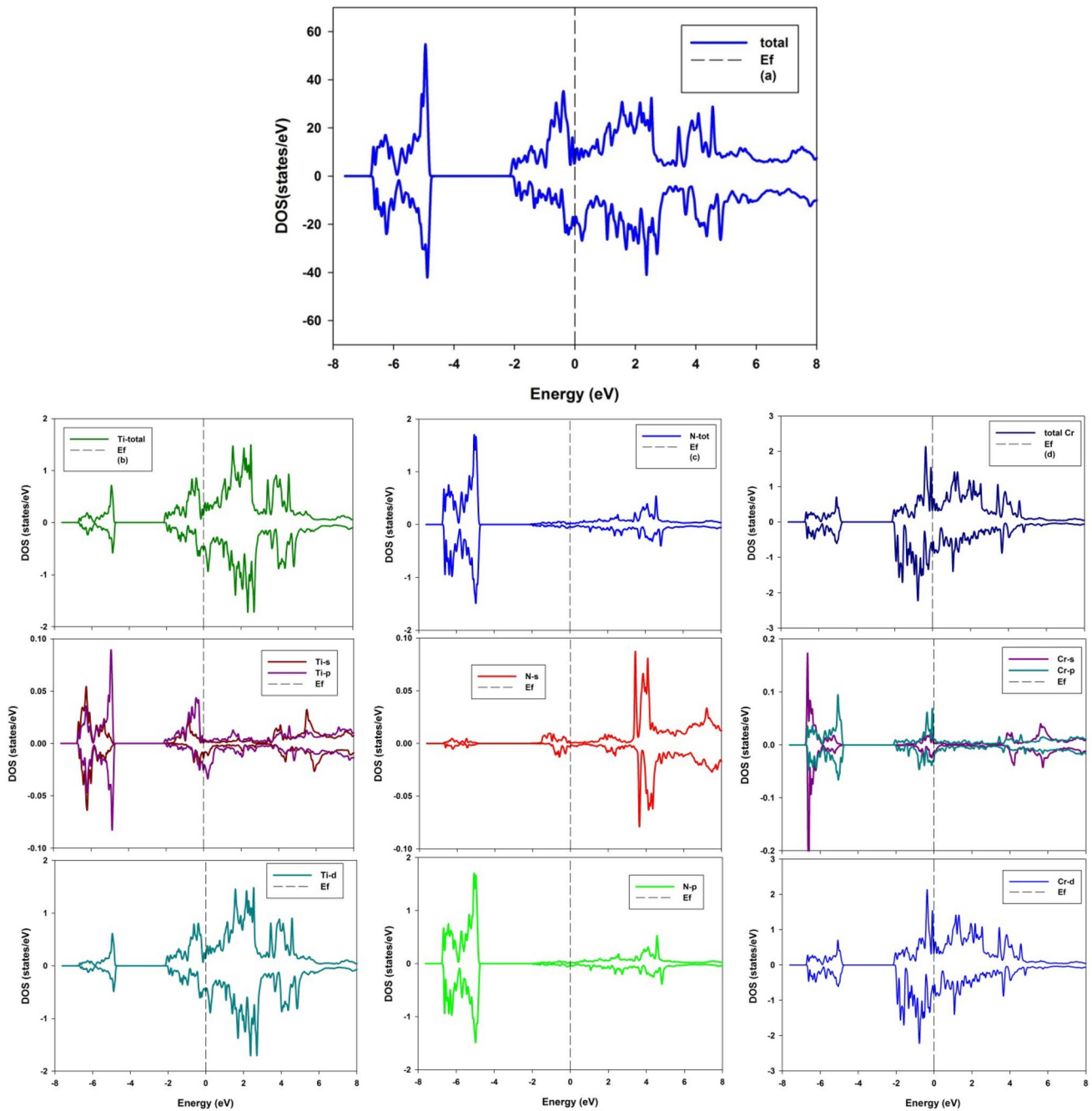


Fig. 3 a The Ti₂N:Cr GL total DOS and b–d partial DOS of its atoms versus energy

$$\text{Im}\epsilon_{ij}^{[\text{inter}]}(\omega) = \frac{\hbar^2 e^2}{\pi m^2 \omega^2} \sum_n \int dk \psi_k^{C_n} |P^i | \psi_k^{V_n} \psi_k^{V_n} | P^j | \psi_k^{C_n} d(E_k^{C_n} - E_k^{V_n} - \omega), \tag{1}$$

where P refers to momentum operator.

The real part of the dielectric function that results from $\text{Im} \epsilon(\omega)$ is defined as follows:

$$\text{Re}\epsilon_{ij}^{[\text{inter}]}(\omega) = \delta_{ij} + \frac{2}{\pi} P \int_0^\infty \frac{\omega' \text{Im}\epsilon_{ij}(\omega')}{(\omega')^2 - \omega^2} d\omega'. \tag{2}$$

In the intraband transitions, $\text{Im } \epsilon(\omega)$ and $\text{Re } \epsilon(\omega)$ are corrected to the following form:

$$\text{Im } \epsilon_{ij}^{[\text{intra}]}(\omega) = \frac{\Gamma \omega_{\text{pl},ij}^2}{\omega(\omega^2 + \Gamma^2)}, \tag{3}$$

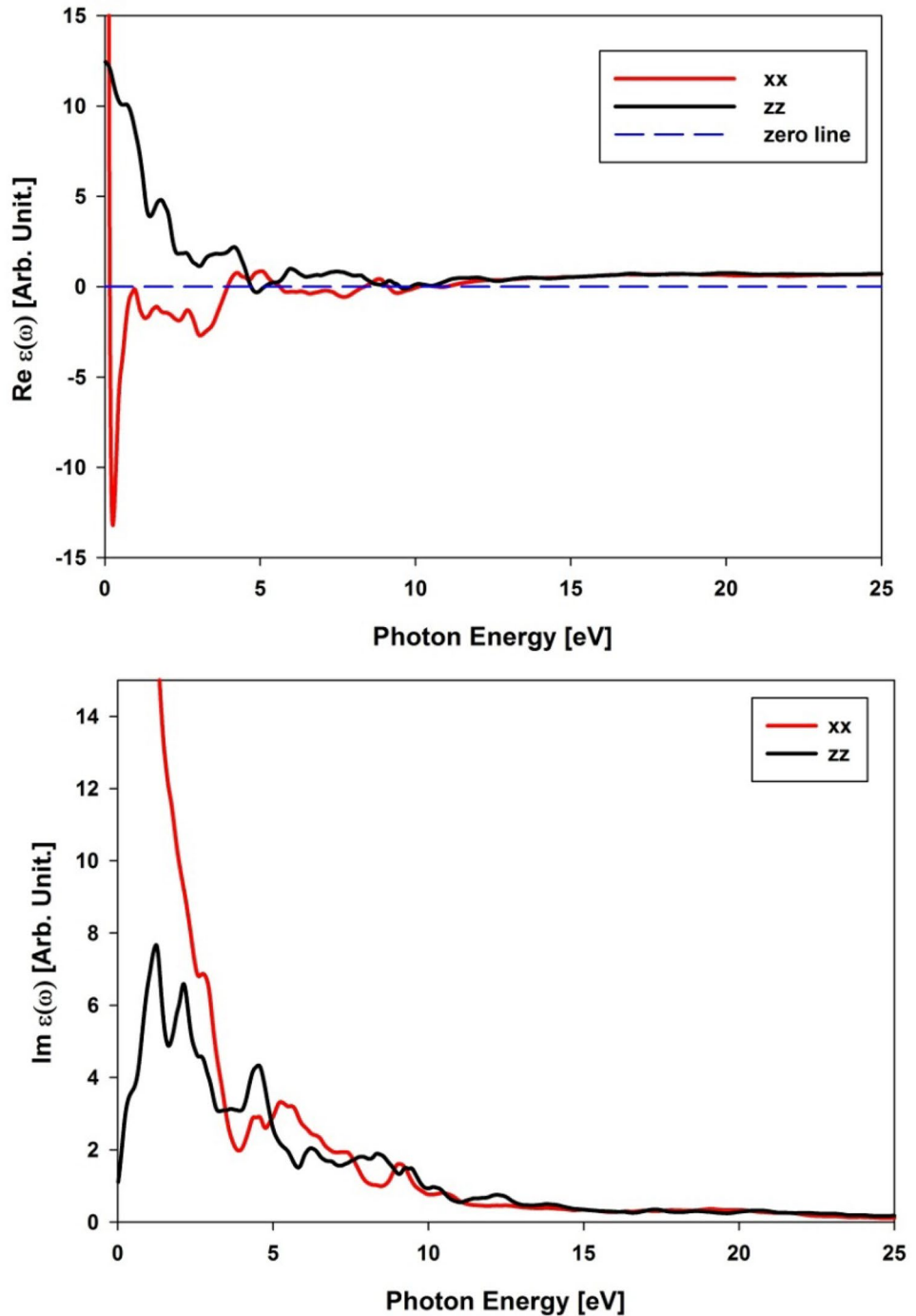
$$\text{Re } \epsilon_{ij}^{[\text{intra}]}(\omega) = 1 - \frac{\omega_{\text{pl},ij}^2}{\omega(\omega^2 + \Gamma^2)}, \tag{4}$$

$$\omega_{\text{pl}}^2 = \frac{ne^2}{\epsilon_0}, \tag{5}$$

where Γ demonstrates the lifetime broadening in the Drude model and ω_{pl}^2 denotes the plasma frequency and n is the electron density.

The total dielectric function includes the inter- and intra-band terms obtained as follows:

Fig. 4 The real and imaginary parts of dielectric function of the $\text{Ti}_2\text{N:Cr}$ GL along the two xx - and zz -directions versus photon energy



$$\varepsilon(\omega) = \varepsilon^{\text{[intra]}}(\omega) + \varepsilon^{\text{[inter]}}(\omega). \quad (6)$$

Re $\varepsilon(\omega)$ and Im $\varepsilon(\omega)$ of the $\text{Ti}_2\text{N}:\text{Cr}$ GL have been shown in Fig. 4 versus photon energy. Based on the two-dimensional (2D) geometry of the $\text{Ti}_2\text{N}:\text{Cr}$ sheet, two directions for the incident light were selected as xx and zz which are in-plane and perpendicular to the sheet. Re $\varepsilon(\omega)$ is optical response tensor to the incident light. It is shown that Re $\varepsilon(\omega)$ has anti-symmetric behavior versus the incident light angle, especially in lower energies (infrared, visible and ultra violet edge). The static value of Re $\varepsilon(\omega)$ (Re $\varepsilon(0)$) is shifted toward the infinite positive value along the xx -direction and is 13 along zz -direction, implying the very high metallic nature of this compound, especially along xx . By increasing photon energy, Re $\varepsilon(\omega)$ - xx dropped dramatically in the infrared region which indicated the optical instability of this direction, reached moderate behavior in the visible area and then shifted to the low amount after 5 eV. But the optical response along the zz -direction has stability and by increasing the photon energy, its amount is slightly decreased towards the ultraviolet edge and at the higher energies, the optical response reached convergence for the two mentioned directions. Based on the metallic behavior of the $\text{Ti}_2\text{N}:\text{Cr}$ GL, Re $\varepsilon(\omega)$ has several roots for the two directions which maybe originated from the plasmonic oscillations. Compared to the pure case [37], the main effect of adding Cr impurity to the Ti_2N GL occurred along the xx -direction in the infrared energy, so that the Re $\varepsilon(\omega)$ sign is changed from negative to positive at zero and also its peak in the visible area is shifted to the negative area. These effects originated by increasing the metallic nature by adding the Cr atom to the Ti_2N GL structure.

The Im $\varepsilon(\omega)$ contains important information about the electronic structure of the materials; each Im $\varepsilon(\omega)$ peak indicates the optical transition of the occupied to unoccupied levels. It indicates the anisotropic behavior of the Im $\varepsilon(\omega)$ at the lower energies for the two mentioned directions. The Im $\varepsilon(\omega)$ is shifted to the infinite amount at zero energy which is due to the high metallic nature of this compound along the xx -direction but by increasing photon energy, it dropped dramatically. Along the zz -direction, we see a difference; its amount is increased from zero in the visible area and then decreased by applying photon energy. The main Im $\varepsilon(\omega)$ peaks of the two mentioned directions are located in the lower energies which originated from the full Ti- and Cr- d orbitals to Ti- and Cr- d ones and then N- p orbital transitions, compared with the DOS diagram. After 10 eV, the real and imaginary parts of dielectric function have been shifted towards zero amount which shows the transparent behavior of this composition for two light accidents. It should be noted that the $\text{Ti}_2\text{N}:\text{Cr}$ GL optical response depends on the angle of the incident light. By comparing the Im $\varepsilon(\omega)$ to the last publications in the pure case, it is shown that the peaks

are increased especially along the zz cases which belong to optical transitions of the Cr- d orbitals [37]. Based on the metallic nature of the $\text{Ti}_2\text{N}:\text{Cr}$ nano-sheet, its optical absorptions occurred in the IR region which makes it a suitable case for optical sensing in this optical area.

Another important optical parameter of the $\text{Ti}_2\text{N}:\text{Cr}$ GL is the Eloss which shows the photon energy loss in the matter (See Fig. 5). The main Eloss diagrams for the mentioned directions have occurred at the 10–15 eV interval energy, while the dielectric functions in this energy range are very low, so it can be seen that the $\text{Ti}_2\text{N}:\text{Cr}$ GL is a good optical sensor by minimum Eloss at the infrared and visible areas. The Re $\varepsilon(\omega)$ has several roots along the xx - and zz -directions in the energies as 0.5, 4.1, 5.9, 8, 9.2, 10.1, 10.5, 13 eV and 4.9, 5.2, 10.1 eV, respectively, but the main Eloss peaks occurred at 4.1, 8, 10.1, 13 eV for xx -direction and 5.2, 8, 10.1 eV for zz -direction, which show the plasmonic energies (Figs. 5, 6).

The absorption diagrams for the $\text{Ti}_2\text{N}:\text{Cr}$ GL of the in-plane and perpendicular directions have been depicted in the Fig. 6. The absorptions are increased significantly in the infrared and visible areas compared to the dielectric functions which indicated that this compound is a good candidate for infrared sensors. By comparing with the pure case, it is shown that added Cr has led to increased absorption in the infrared region. Based on the lower amount of the Eloss in the lower optical energies, this compound is suitable for IR sensors.

The refraction and extinction diagrams are shown in Fig. 7 versus photon energy. The refraction index has infinite amount at zero energy which originated from the high metallic behavior of the d orbitals along xx -direction, but has the finite refraction about 3.5 which is referred to the semiconducting nature. By increasing the photon energy, the refraction dropped dramatically along xx which denoted the optical instability in the infrared region. At higher energies (up to 10 eV) the two painted refractions are shifted to one and lower of it, which implied the super luminance phenomena that the light velocity is higher than vacuum amount.

The zz diagram is dropped with slight slope and after visible area the $\text{Ti}_2\text{N}:\text{Cr}$ GL has the insulator conduct. Based on the high metallic nature of the $\text{Ti}_2\text{N}:\text{Cr}$ GL at lower energies and existence of the half-full d orbitals, the extinction variations are very intense and we see high absorption in the infrared area along xx , but zero amount for zz -direction which indicated the semiconducting behavior. After 10 eV, all extinctions are very low which indicated the transparent treatment of this composition. After 10 eV, the refraction index is lower than 1 which seems to exceed the group velocity of the electromagnetic waves in the matter than light velocity.



Fig. 5 The Eloss function versus photon energy of the *xx*- and *zz*-directions

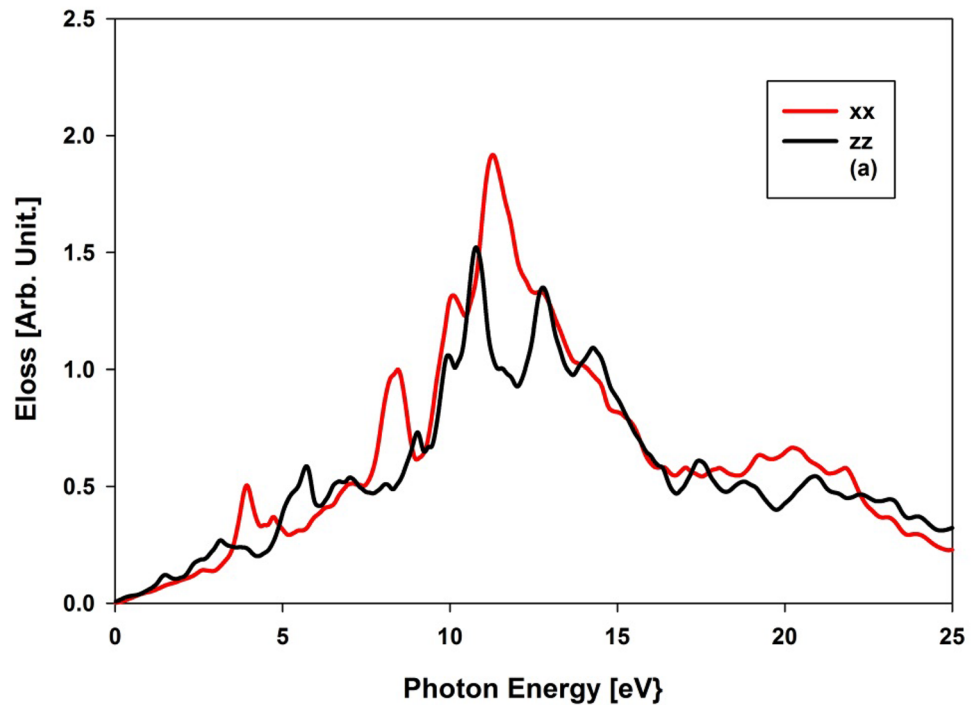
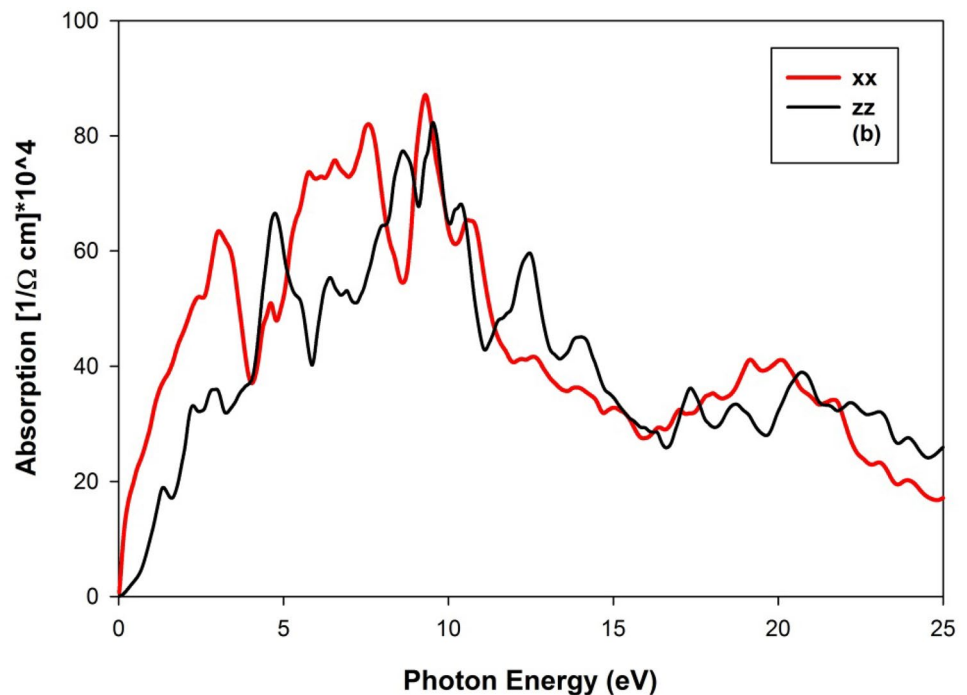


Fig. 6 The absorption diagram of the $\text{Ti}_2\text{N:Cr}$ GL along the two *xx*- and *zz*-directions versus photon energy



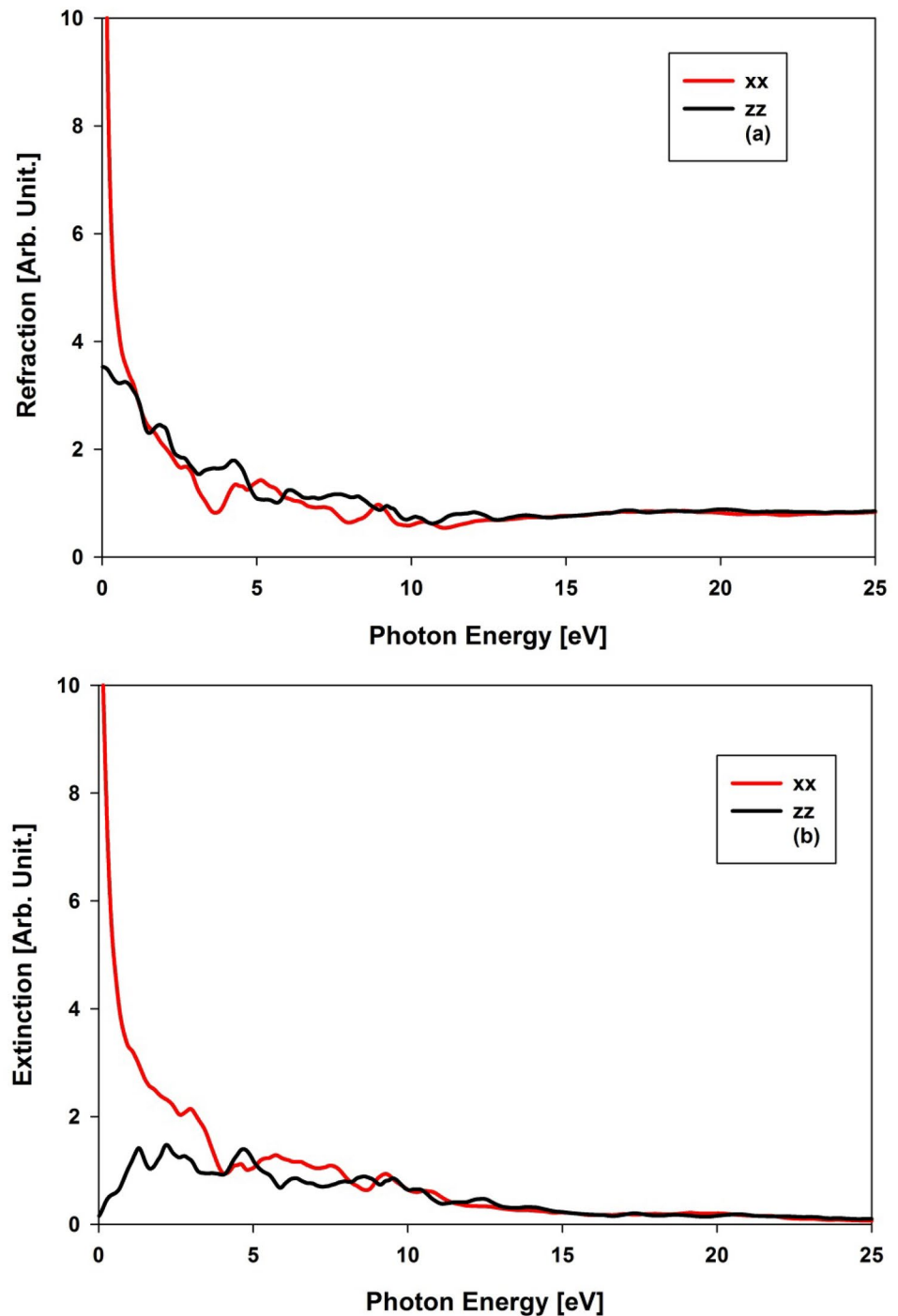
Conclusions

The Cr impurity was replaced in the Ti site in the Ti_2N GL and the electronic and optical calculations were done based on DFT framework by FP-LAPW method. $\text{Ti}_2\text{N:Cr}$ GL was found to show magnetic behavior; therefore,

the electronic structure in the two up and down spins is different. Increasing the density around the Fermi level has caused an increase in electron mobility. The optical response of our compound has a red shift than the pure case. Also, the optical behavior has the anisotropy conduct in the infrared and visible areas. The main optical response at the *xx*- and *zz*-directions occurred in the lower



Fig. 7 The refraction and extinction diagram of the $\text{Ti}_2\text{N:Cr}$ GL along the two xx - and zz -directions versus photon energy



energies but the Eloss magnitudes are in the ultraviolet region, so this composition is a good candidate for infrared sensors. By adding the Cr impurity to this nano-sheet, the $\text{Im } \epsilon(\omega)$ peaks are increased which referred to the Cr- d orbital transitions. The metallic nature is increased along the xx -direction and along the zz has semi-metallic behavior in the lower energies but at higher energies reached

the insulating behavior and symmetry along the two mentioned directions. Also, the light phase velocity is higher than its amount in the vacuum in the higher energies of ultraviolet range.

Open Access This article is distributed under the terms of the Creative Commons Attribution 4.0 International License (<http://creativecommons.org/licenses/by/4.0/>), which permits unrestricted use,



distribution, and reproduction in any medium, provided you give appropriate credit to the original author(s) and the source, provide a link to the Creative Commons license, and indicate if changes were made.

References

- Novoselov, K.S., Geim, A.K., Morozov, S.V., Jiang, D., Katsnelson, M.I., Grigorieva, A.V., Dubonos, S.V., Firsov, A.A.: Two-dimensional gas of massless Dirac fermions in graphene. *Nature* **438**, 197 (2005)
- Ma, F., Jiao, Y., Gao, G., Gu, Y.T., Bilic, A., Chen, Z., Du, A.: Graphene-like two-dimensional ionic boron with double Dirac cones at ambient condition. *Nano Lett.* **16**, 3022 (2016)
- Wang, A.J., Li, H., Huang, H., Qian, Z.S., Feng, J.: Fluorescent graphene-like carbon nitrides: synthesis, properties and applications. *J. Mater. Chem. C* **4**, 8146 (2016)
- Mhamane, D., Aravindan, V., Kim, M.S., Kim, H.K., ChulRoh, K., Ruan, D., Lee, S.H., Srinivasan, M., Kim, B.: Silica-assisted bottom-up synthesis of graphene-like high surface area carbon for highly efficient ultracapacitor and Li-ion hybrid capacitor applications. *J. Mater. Chem. A* **4**, 5578 (2016)
- Lashgari, H., Boochani, A., Shekaari, A., Solaymani, S., Sartipi, E., Mendi, R.T.: Electronic and optical properties of 2D graphene-like ZnS: DFT calculations. *Appl. Surf. Sci.* **369**, 76 (2016)
- Huang, Y., Guo, J., Kang, Y., Ai, Y., Ming Li, C.: Two dimensional atomically thin MoS₂ nanosheets and their sensing applications. *Nanoscale* **7**, 19358 (2015)
- Krainara, N., Limtrakul, J., Illas, F., Bromley, S.T.: Structural and electronic bistability in ZnS single sheets and single-walled nanotubes. *Phys. Rev. B* **83**, 233305 (2011)
- Crepaldi, A., Autès, G., Sterzi, A., Manzoni, G., Zacchigna, M., Cilento, F., Vobornik, I., Fujii, J., Bugnon, P., Magrez, A., Berger, H., Parmigiani, F., Yazyev, O.V., Grioni, M.: Persistence of a surface state arc in the topologically trivial phase of MoTe₂. *Phys. Rev. B* **95**, 041408(R) (2017)
- Deng, X., Sorescu, D.C., Lee, J.: Single-layer ZnS supported on Au(111): A combined XPS, LEED, STM and DFT study. *Surf. Sci.* **658**, 9 (2017)
- Ma, Y., Wang, Y., Oganov, A.R.: Absence of superconductivity in the high-pressure polymorph of MgB₂. *Phys. Rev. B* **79**, 054101 (2009)
- Boochani, A., Nowrozi, B., Khodadadi, J., Solaymani, S., Jalali-Asadabadi, S.: Novel graphene-like Co₂VAL (111): Case study on magnetoelectronic and optical properties by first-principles calculations. *J. Phys. Chem. C* **121**, 3978 (2017)
- Bostwick, A., McChesney, J., Ohta, T., Rotenberg, E., Seyller, T., Horn, K.: Experimental studies of the electronic structure of graphene. *Progr. Surf. Sci.* **84**, 380 (2009)
- Schilling, M. B., Schoop, L. M., Lotsch, B. V., Dressel, M., and Pronin, A. V.: Gate-induced localized states in graphene: Topological nature in their formation. *Phys. Rev. B* **98**, 235427 (2018)
- Soldano, C., Mahmood, A., Dujardin, E.: Production, properties and potential of graphene. *Carbon* **48**, 2127 (2010)
- Kuilla, T., Bhadra, S., Yao, D., Kim, N.H., Bose, S., Lee, J.P.: Recent advances in graphene based polymer composites. *Progr. Polym. Sci.* **35**, 1350 (2010)
- Molitor, F., Guttinger, J., Stampfer, C., Droscher, S., Jacobsen, A., Ihn, T., et al.: Electronic properties of graphene nanostructures. *J. Phys. Condens. Matter* **23**, 243201 (2011)
- Rozhkov, A.V., Giavaras, G., Bliokh, Y.P., Freilikher, V., Nori, F.: Electronic properties of mesoscopic graphene structures: Charge confinement and control of spin and charge transport. *Phys. Rep.* **503**, 77 (2011)
- Singh, V., Joung, D., Zhai, L., Das, S., Khondaker, S.I., Seal, S.: Graphene based materials: Past, present and future. *Progr. Mater. Sci.* **56**, 1178 (2011)
- Naguib, M., Kurtoglu, M., Presser, V., Lu, J., Niu, J., Heon, M., Hultman, L., Gogotsi, Y., Barsoum, M.W.: Two-dimensional nanocrystals produced by exfoliation of Ti₃AlC₂. *Adv. Mater.* **23**, 4248–4253 (2011)
- Shein, I.R., Ivanovskii, A.L.: Graphene-like titanium carbides and nitrides Ti_{n+1}C_n, Ti_{n+1}N_n (n = 1, 2, and 3) from de-intercalated MAX phases: First-principles probing of their structural, electronic properties and relative stability. *Comput. Mater. Sci.* **65**, 104–114 (2012)
- Enyashin, A.N., Ivanovskii, A.L.: Structural, electronic properties and stability of MXenes Ti₂C and Ti₃C₂ functionalized by methoxy groups. *Comput. Theor. Chem.* **989**, 27–32 (2012)
- Zhang, Z., Liu, X., Yakobson, B.I., Guo, W.: Two-dimensional tetragonal TiC monolayer sheet and nanoribbons. *J. Am. Chem. Soc.* **134**, 19326–19329 (2012)
- Tang, Q., Zhou, Z., Shen, P.: Are MXenes promising anode materials for Li Ion batteries? computational studies on electronic properties and Li storage capability of Ti₃C₂ and Ti₃C₂X₂ (X = F, OH) monolayer. *J. Am. Chem. Soc.* **134**, 16909–16916 (2012)
- Naguib, M., Mashtalir, O., Carle, J., Presser, V., Lu, J., Hultman, L., Gogotsi, Y., Barsoum, M.W.: Two-dimensional transition metal carbides. *ACS Nano* **6**, 1322–1331 (2012)
- Enyashin, A.N., Ivanovskii, A.L.: Structural and electronic properties and stability of MXenes Ti₂C and Ti₃C₂ functionalized by methoxy groups. *J. Phys. Chem. C* **117**, 13637–13643 (2013)
- Shein, I.R., Ivanovskii, A.L.: Planar nano-block structures Ti_{n+1}Al_{0.5}C_n and Ti_{n+1}C_n (n = 1, and 2) from MAX phases: Structural, electronic properties and relative stability from first principles calculations. *Superlattices Microstruct.* **52**, 147–157 (2012)
- Barsoum, M.W.: The M_{N+1}AX_N phases: A new class of solids: Thermodynamically stable nanolaminates. *Prog. Solid State Chem.* **28**, 201–281 (2000)
- Högberg, H., Hultman, L., Emmerlich, J., Joelsson, T., Eklund, P., Molina-Aldareguia, J.M., Palmquist, J.P., Wilhelmsson, O., Jansson, U.: Growth and characterization of MAX-phase thin films. *Surf. Coat. Technol.* **193**, 6–10 (2005)
- Barsoum, M.W., El-Raghy, T.: Synthesis and characterization of a remarkable ceramic: Ti₃SiC₂. *J. Am. Ceram. Soc.* **79**, 1953–1956 (1996)
- Verger, L., Xu, C., Natu, V., Cheng, H.-M., Ren, W., Barsoum, M. M.: Overview of the synthesis of MXenes and other ultrathin 2D transition metal carbides and nitrides. *Curr. Opin. Solid State Mater. Sci.* **23**, 149–163 (2019)
- Come, J., Naguib, M., Rozier, P., Barsoum, M.W., Gogotsi, Y., Taberna, P.-L., Morcrette, M., Simon, P.: A non-aqueous asymmetric cell with a Ti₂C-based two-dimensional negative electrode. *J. Electrochem. Soc.* **159**, A1368–A1373 (2012)
- Jiang, J.-X., Jin, S., Wang, Z.-H., Tan, C.-L.: Electronic structure and optical properties of layered ternary carbide Ti₃AlC₂. *Chin. Phys. Lett.* **28**, 037101 (2011)
- Wang, X.H., Zhou, Y.C.: Layered machinable and electrically conductive Ti₂AlC and Ti₃AlC₂ ceramics: a review. *J. Mater. Sci. Technol.* **26**, 385–416 (2010)
- Wu, M., Guo, J., Li, Y., Zhang, Y.: Esterification of benzoic acid using Ti₃AlC₂ and SO₄²⁻/Ti₃AlC₂ ceramic as acid catalysts. *Ceram. Int.* **39**, 9731–9736 (2013)
- Wang, J., Zhou, Y., Liao, T., Zhang, J., Lin, Z.: A first-principles investigation of the phase stability of Ti₂AlC with Al vacancies. *Scr. Mater.* **58**, 227–230 (2008)
- Rao, J.C., Pei, Y.T., Yang, H.J., Song, G.M., Li, S.B., De Hosson, J.T.M.: TEM study of the initial oxide scales of Ti₂AlC. *Acta Mater.* **59**, 5216–5223 (2011)



37. Lashgari, H., Abolhassani, M.R., Boochani, A., Elahi, S.M., Khodadadi, J.: Electronic and optical properties of 2D graphene-like compounds titanium carbides and nitrides: DFT calculations. *Solid State Commun.* **195**, 61–69 (2014)
38. Wang, S., Li, J.-X., Du, Y.-L., Cui, C.: First-principles study on structural, electronic and elastic properties of graphene-like hexagonal Ti_2C monolayer. *Comput. Mater. Sci.* **83**, 290–293 (2014)
39. Xie, Y., Naguib, M., Mochalin, V.N., Barsoum, M.W., Gogotsi, Y., Yu, X., Nam, K.-W., Yang, X.-Q., Kolesnikov, A.I., Kent, P.R.C.: Role of surface structure on Li-ion energy storage capacity of two-dimensional transition-metal carbides. *J. Am. Chem. Soc.* **136**, 6385–6394 (2014)
40. Come, J., Naguib, M., Rozier, P., Barsoum, M.W., Gogotsi, Y., Taberna, P.L., Morcrette, M., Simon, P.: A non-aqueous asymmetric cell with a Ti_2C -based two-dimensional negative electrode. *J. Electrochem. Soc.* **159**, A1368–A1373 (2012)
41. Solaymani, S., Ghaderi, A., Beryani, N.: Comment on: Characterization of microroughness parameters in titanium nitride thin films grown by DC magnetron sputtering. *J. Fusion Energy* **31**(6), 591 (2012)
42. Țălu, Ș., et al.: Micromorphology analysis of specific 3-D surface texture of silver chiral nanoflower sculptured structures. *J. Ind. Eng. Chem.* **43**, 164 (2016)
43. Țălu, Ș., et al.: Fractal features of carbon–nickel composite thin films. *Microsc. Res. Tech.* **79**(12), 1208 (2016)
44. Țălu, Ș., et al.: Microstructure of nickel nanoparticles embedded in carbon films: case study on annealing effect by micromorphology analysis. *Surf. Interface Anal.* **49**(3), 153 (2017)
45. Zare, M., et al.: Evolution of rough-surface geometry and crystalline structures of aligned TiO_2 nanotubes for photoelectrochemical water splitting. *Sci. Rep.* **8**(1), 10870 (2018)
46. Blaha, P., Schwarz, K., Sorantin, P., Trickey, S.B.: Full-potential, linearized augmented plane wave programs for crystalline systems. *Comput. Phys. Commun.* **59**, 399 (1990)
47. Blaha, P., Schwarz, K., Madesen, G.K.H., Kvasnicka, D., Luitz, J.: WIEN2K an augmented plane wave +local orbitals program for calculating crystal properties. Karlheinz Schwarz. Techn; Universitaetwien, Wein (2001)
48. Perdew, J., Chevary, J.A., Vosko, S.H., Jackson, K.A., Pederson, M.R., Singh, D.J., Fiolhais, C.: Atoms, molecules, solids, and surfaces: applications of the generalized gradient approximation for exchange and correlation. *Phys. Rev. B* **46**, 6671 (1992)
49. Fox, A.M.: *Optical Properties of Solids*. Oxford University Press, Oxford (2001)
50. Wooten, F.: *Optical Properties of Solids*. Academic Press, New York (1972)

Publisher's Note Springer Nature remains neutral with regard to jurisdictional claims in published maps and institutional affiliations.

